Chapter

Uniaxial and Triaxial Creep Performance of Calcarenitic and Sandy Oolitic Limestone Formations for Stability Analysis of Roman Rock-Cut Tombs in Alexandria, Egypt

Sayed Hemeda

Abstract

The Greek-Roman rock-cut tombs at Alexandria, Egypt, were excavated mainly in the calcarenitic limestone formations and show varying degrees of damage of rock pillars and ceilings. In order to understand the long-term rock mass behaviour in selected tombs and its impact on past failures and current stability, uniaxial and triaxial Creep tests and rock mass quality assessments had been carried out. Creep behavior of rock plays an important role in underground works, especially for archeological structures subjected to large initial stresses. These conditions yield nonreversible deviatoric creep strains that develop during time at constant stress. In order to describe the time-dependent deformation, various approaches have been established based on analytical, empirical, and numerical methods. Our analyses show that the Roman tombs at Alexandria have been cut into poor quality rock masses. Rock failures of ceilings and pillars were frequently facilitated by local, unfavourably oriented persistent discontinuities, such as tension cracks and joints. Other failures were related to the disintegration of calcarenitic and oolitic limestones. Our data suggest that, in Roman age monumental tomb construction, low-strength rock masses resulted in modifications of the planned tomb design in order to minimise the risk of rock falls and to prevent collapses.

Keywords: Roman rock-cut tombs, geotechnical assessment, creep tests, calcarenitic limestone, oolitic limestone, rock mass rating, tomb construction

1. Introduction

Creep is an irreversible ductile time-dependent deformation, without fracture where deformation does not occur suddenly when applying stress as opposed to brittle fracture. Instead, strain accumulates as a result of long-term stress [1–4]. This behavior usually distinguishes weak rocks such as rock salt, shale, buttocks, venetian, silt, and sandstone. Rock creep behavior has been widely discussed in the

literature, based on experimental results from laboratory or field investigations, foundational modeling, and numerical analyses. The main objective of this chapter is to focus on appropriate methodologies for determining the creep behavior of soft/weak intact rocks through laboratory experimental analysis and critical evaluation of available rheological models to explain creep behavior [5–9].

Creeping in fragile hard rocks is rare because the deformation rate is too slow. Solid rocks exhibit a creep behavior noticeably only at elevated temperatures and pressures generally not encountered in engineering structures. Soft rocks on the other hand mostly creep at room temperature, atmospheric pressure, and the range of deviating stress typically encountered in engineering structures [10–12].

As we know, creeping rocks have a significant effect on the long-term stability of the rocks and the surrounding surface [13–16]. For broken rocks, porosity is the primary determinant of creep characteristics, but in the existing literature, the stress rate was mainly used to describe the creeping properties of broken rocks. For example, Wang [17, 18] carried out numerical simulations on the process of creeping damage to the road surrounding the rock under high pressure, and Zhu and Ye discussed the law of creep affected by water content by comparing the results of the rock creep test under dry condition and in saturation. Zhang and Luo [19] studied the properties of creeping rocks under different stress levels. Liu et al. [20] performed triaxial creep tests on coal and rock by step loading method. Zhang and Luo [19] examined the creeping test of marble and soft rock separately; Parkin [21] used a pressure meter to study the rheological properties of granular materials. Shen and Zhao [22] proposed a model for three parameters of creeping rock filling through rheological experiments on limestone. Zheng and Ding proposed a creep model to rocks of nine parameters and obtained parameter indexes through tests. Guo et al. [23] proposed a modified three-parameter rheological model for coarse-grained materials. Wang [24] and Liu et al. [25] summarized the rheological state of coarse-grained materials and noted that experimental studies on granular materials were insufficient.

They suggested that it is necessary to study the mechanism of partial deformation of coarse granular materials given the effect of the scale for internal testing.

Understanding the mechanisms of deterioration of the calcarenite rock structures in which the Greco-Roman monuments are excavated requires a comprehensive study of the mechanical behavior and engineering properties of the calcarenite rocks. In addition to geological and geomorphological concerns, numerous investigations have been conducted on rock degradation and disintegration. As the areas are an open museum and attractive places for tourists, sampling can only take place in a limited number of locations with official permission. For this purpose, cylindrical samples with a diameter of 42–44 mm and a height of 90–100 mm, prepared using a basic drilling machine and some blocks collected from archeological sites under investigation (catacomb from Kom El-Shoqafa, El-Shatby tombs, and tombs of Mustafa Kamel), as shown in **Figure 1** illustrates the physical, short, and long-term mechanical properties of calcarenitic rocks in the laboratory, a number of samples prepared from these blocks have been used for testing, and the limitations of the number of blocks have been overcome by determining the topical properties of the rocks through hammer tests. Schmidt, pictorial geographic investigations and classification of the rocky hill in some outcrops and in some rock structures where testing was permitted.

The purpose of this research is to make recommendations on the strengthening and safety of archeological underground structures under long- and short-term loading. For this purpose, a set of experimental tests and advanced digital analyses had been performed.

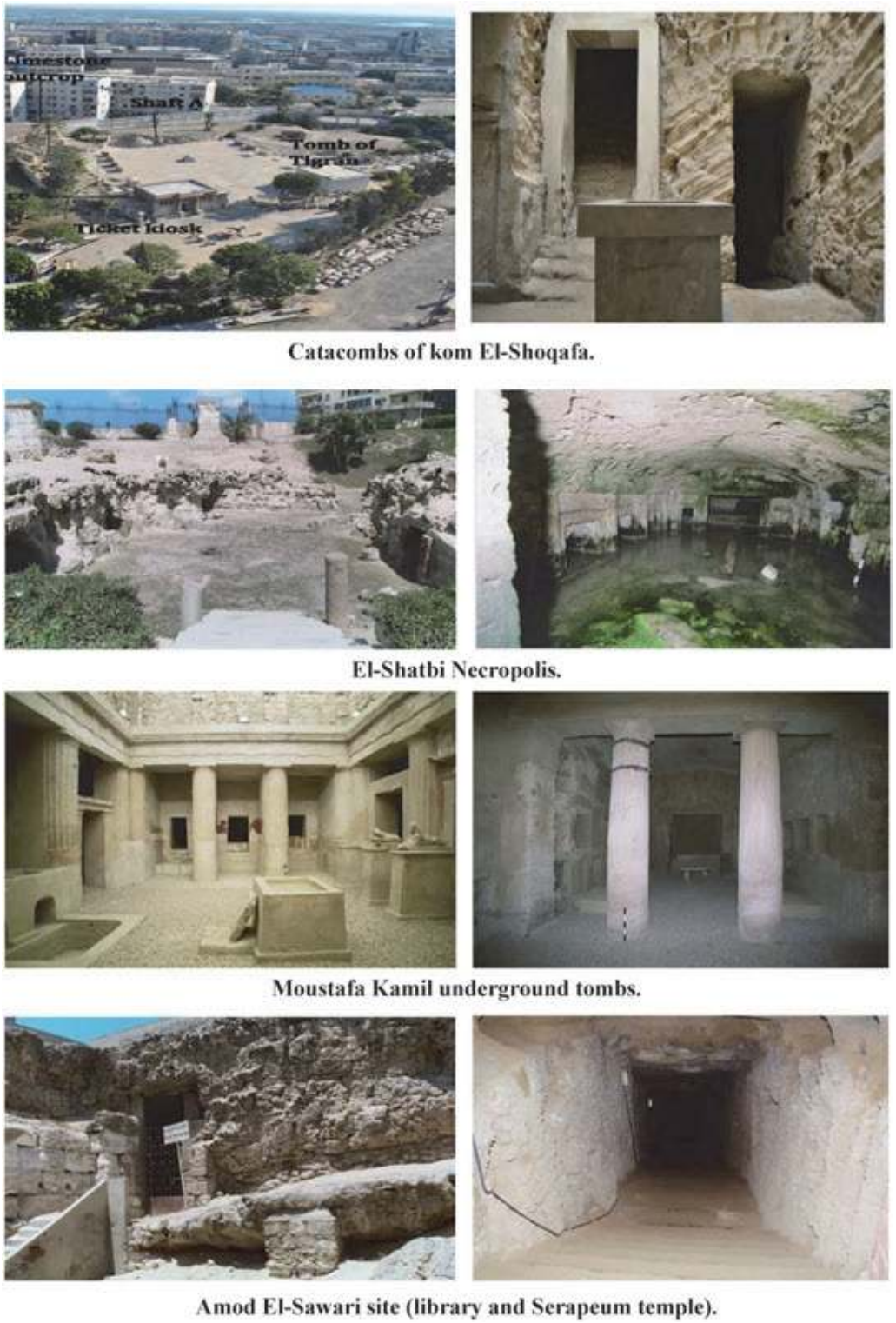

Figure 1.
Underground monuments (Catacombs) in Alexandria, (present conditions).

Calcarenitic rocks and other type of fine limestone (under investigations) are porous rocks with complex behavior [26–28]. Two major mechanisms can be identified to distort types of rock properties, depending on conditions in-situ stress: (1) the prevalence of fracture, associated with volumetric expansion and fragile

behavior, which is predominant in compressive stress paths in the absence of low confined pressure, or (2) pore breakdown, which dominates high-stress conditions, producing plastic deformations and large contracting [29].

The high fossil content, mainly due to the shells of necrosis and some mollusks, leads to structural heterogeneity, which is reflected in the variance of mechanical properties and weaknesses in the conclusion of experimental results [13].

There is no generally accepted theory of fragile rock strength based on examination of the process of formation of microcracks and deformation, and the establishment of the initiation and development of stress-induced fractures in EDZ is therefore a major concern.

Some of the main concerns related to the stability of underground structures in soft rocks include the effects of potential land disturbances through the method of drilling and reallocation of pressures at the site surrounding the excavations [30–35]. Each of these factors relates to the initiation and spread of fragile fractures and the extent of the troubled drilling area (EDZ), which can adversely affect the stability of the drilling boundaries and can increase the permeability of host rocks to the near field. In structural and tectonic geology, experimental rock deformation is important in determining the evolution of natural structures and tectonic features [36, 37].

Great effort has been made toward understanding the fragile fracture processes and mechanisms. Much of this focus extended to laboratory tests and quantification/measurement of fragile fracture thresholds [7, 38]. Among these, damaged thresholds marked by the onset of expansion, which is the reflection point of the volumetric pressure curve, are particularly important because many studies have linked the threshold to the spread of unstable fracture in fragile rocks [7]. The unstable crack spreading corresponds to the point where the reproduction process is controlled between the applied stress and the speed of crack growth. Under these circumstances, the crack will continue to spread until failure even if the applied load stops and remains stable. As such, Martin and Chandler and Read et al. equated the threshold of damage caused by cracking and the long-term on-site strength of fragile rocks.

Thus, the identification of these processes and associated mechanisms is essential in predicting both the strength of soft rocks in the short and long term. This research focuses on these processes by presenting the results of many short- and long-term laboratory tests.

In general, the spread of cracks can be equated with the irreversible destruction of molecular cohesion along the path of the crack generated. In this sense, the miniature crushing process "damages" the rock material. Due to the multiplication of the number of reproductive fractures, the damage can be considered to be cumulative and can be associated with a perceived lack of elastic stiffness and the strength of material cohesion.

In this work, we highlighted some important characteristics of the geotechnical behavior of structured soft rocks and showed that these properties are very common in many natural rocks. Based on these concepts, research into soil/rocky transition material has intensified in the last two decades [39].

2. Geological and tectonic setting

The Roman underground tombs in Alexandria are located on the northern edge of the "Nile Delta geomorphic province, c. 1.30 km north of the Lake Maryout and 1.42 km south of the Mediterranean Sea shoreline, as shown in **Figure 2**". Since Pleistocene time, within the last 1 million years, Lake Maryout has intermittently

Figure 2.
The limestone outcrop at the catacombs of Kom El-Shoqafa.

been connected to fresh Nile river flows and sea water sources and has been both at and below mean sea level. Lake Maryout and Delta had varied depositional environment, including "silt and clay deposits with some organics (lagoonal deposit)"; "sand and silt deposits (Nile River deposits); "sand deposits (beach and littoral deposits"). The basement rock unit is Miocene (6–25 million years old) and older carbonate formations that comprise the Egyptian plateau. Above the Miocene sedimentary rocks are Plio-Pleistocene age (less than 6 million years old) sediments consisting of alternating beds of shale, limestone, sandstone, silt, and calcareous sand.

The Plio-Pleistocene sediments form a series of ridge and trough that are approximately parallel to the Mediterranean coastline in the vicinity of the catacomb site. Most of the city of Alexandria rests on one of these topographic ridges while behind the ridge, Lake Maryout is in a trough. The near surface limestone deposits, which are commonly encountered in the Alexandrian ridge, are cemented marine sand.

3. State of preservation

The catacombs of Alexandria show some clear indications of yield and partial collapse in several locations, as defined in the honeycomb weathering, the contour scaling and spalling of the stone surface, the disintegration of building materials, and the wet surfaces of rocky meals especially for semi-protected parts of the excavation; also, we observe salt flowering and yellow staining of yellow iron in many wall parts.

Structural damage is obvious like the wall cracking, the thinning out of rock pillars, disintegration and degradation of the walls surfaces, the partial collapse of some parts of the roofs and walls, and the peeling of rocks, especially in the roof of narrow corridors found in the deepest parts and mass waste from the ceiling and walls.

In conclusion, the current state of conservation of the great catacombs at Kom El-Shoqafa, the best-known and most famous testimony of the culture of the funerary architecture of Alexandria, is now at its most deteriorating.

Most structural damage is caused by one or a combination of the following factors:

- The gradual weakening of rock materials due to the intrinsic sensitivity of weathering factors, especially the effect of weathering with groundwater and salt
- Earthquake and other man-made dynamic loading
- Permanent deformation of the rock mass
- Natural wear and tear of materials
- History of construction in the area

4. Mineralogical and petrographical studies

The effort behind thin-section analysis was to provide insight into the closed grains (calcite/sand) and/or theories of overgrowth after precipitation of the large angle of internal friction. Due to the fragile nature of the rocks and plaster layers being excavated, it was necessary to be very careful to make thin sections, which were studied using independent polarized light, electron microscopy (SEM), and stereoscopic observation.

A light-transmitted polarized plane, scanning electron microscopy, and stereoscopic observations were used to determine the interlocking textures and connections between grains and crystals. These contacts rely on differences in solubility due to impurities and differences in bending radius, which lead to the penetration of smaller grains in large grains.

In addition, thin section microscopy was used to help explain the large friction angles associated with the material, limestone/rock.

Miniature petrographic description of stones/rocks for engineering purposes includes the identification of all parameters that cannot be obtained from a comprehensive endoscopic examination of rock samples, such as mineral content, grain size and texture, which have an impact on the mechanical behavior of the rock or rock mass. To ensure proper classification, the first step should be to check the metal composition and rock texture; see **Table 1**. Mineralogy summarizes the three types of soft limestone under investigation. Additional investigations should include analysis of the texture and minerals in the case of highly contrasting rocks, determining the degree of change or weathering, grain size, partial fracture, and porosity.

In sandstone, limestone, and calcarenite samples intact, it is possible to determine with the naked eye an alternative sequence of white and pink bands with a

Rock type	Calcite $CaCO_3$ %	Quartz SiO_2 %	Gypsum $CaSO_4.2H_2O$ %	Halite NaCl %	Other %
Sandy oolitic limestone (Kom El-Shoqafa) (COM)	47–65	31–23	10–5	12–9	2
Intact Calcarenite (Mustafa Kamel Necropolis) (M)	52–72	28–18	8–3	12–6	3–5
Oolitic intraclastic limestone (El-Shatby Necropolis) (SH)	53–80	25–20	11–7	11–7	3

Table 1.
Mineralogy of the three soft limestone types under investigation.

thickness of about 1 mm (bedding plane). Optical microscopy and counting points were performed on thin sections of rock samples. The air-dried samples were inoculated with Canada balsam, and the thin sections were then cut perpendicular to the bedding planes. A thin section is observed under parallel light and polarizing light. The following is a detailed analysis of the rock samples collected from the three archeological sites under investigation, rock samples from six collections of El-Shatby with code Nr (SH), five rock samples collected from the tombs of Mustafa Kamel 1 and No. 2 with code Nr (M), and four samples Rock collected from Catacomb of Kom El-Shoqafa code Nr (COM).

4.1 Catacombs of Kom El-Shoqafa

In the internal structure, we can observe the dominant components, which are the cells of the fibers of the stomach, grass, algae, and mother of pearl, mostly with a test wall of microscopic microspheres, while the tests are filled internally with microtomes and microbes (**Figure 3**). Surrounded monocrystalline quartz granules of varying sizes and perimeter of iron oxides have been detected representing the previous presence of K-feldspar grains. Rock and granular materials make up this fossil sand limestone, or cement sand.

(Calcarenite size) 15% of customizations are medium-sized numulite tests filled with prickly calcite. 15% of foraminifers tests with a neomorphic microspar test wall and test chambers are full of neomorphic microspar. 20% of medium size bryoza and algae tests 0.25% small size, monocrystalline, crispy extinction, quartz granules subrounded. 25% medium to small size structure less ooides. Customizations are solidified by isopachous microspar. Porosity is a fit of 20% of the area of the thin-section field, which is reduced by microscopy. Oxidation is observed as red color spots.

4.2 Mustafa Kamel Necropolis

The rock texture in these tombs consists of two textures, namely packed stone and stone. These two types of texture show different proportions and sizes of quartz granules, and different biological plates, especially foraminifer tests. Most Ooides lost their internal structure. Few of them retain their concentric structure. Consolidation of the components of this limestone is represented by isopachous microspar (**Figure 4**).

(Calc rud –arenite size) 58% of the assignments are medium in size, thin and micro pigment and less pollutant internal structure. 10% micritic oval. 30% large to small angular size to subrounded, crispy extinction, monocrystalline quartz. 2% plajioclase and microcline crystals. Porosity reached 20% of the area of the thin-section field. The pores are filled with neomorphic microspar. Allochems are surrounded with isopachous microspar.

Calcarenite is a bio-soft rock originating from marine sediments, which occurred during the overflow and decline of the region in the Ice Age. The calcarenite consists of almost pure calcium carbonate and is applied directly to the limestone rock of the Cretaceous.

4.3 El-Shatby cemetery

Changes in internal structure and metals were analyzed and the most distinctive textures documented on the images. In the internal structure, we can observe the porosity increase of various sizes. In some places, we can find cracks on metal contacts or even inside metals. Generally, significant changes are shown in the cement material; see **Figure 5**. Limestone in this site can be classified into two types

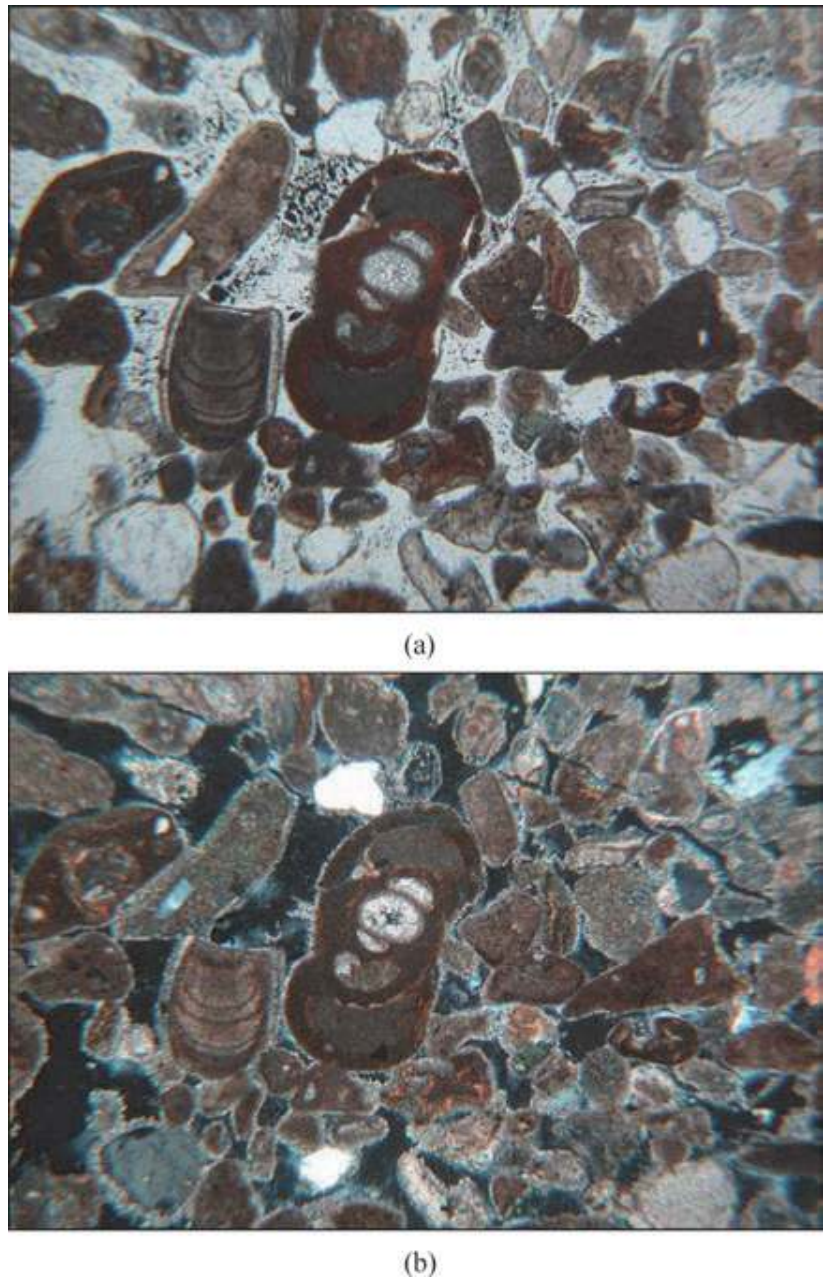

Figure 3.
Photomicrograph of fossiliferous sandy oolitic limestone, (a) under parallel polarized light, (b) under cross polarized light (XPL), showing bioclasts of gastropods, foraminifera, algae, and shell debris; most of them are with test wall of neomorphic microspar, filled with micrite and microspar, cracks between and through the minerals are obvious. Catacombs of Kom El-Shoqafa.

of fabric, namely, fossiliferous oolitic intraclasic limestone. These two types of texture are in different proportions of quartz granules, biological panels, ooides, and peloids.

(Callus arinite rod size) 80% of the customizations are medium-sized structure less ooides. 10% large to medium-sized monocrystalline unite extinction, quartz granules subrounded. 5% large polycrystalline, crispy extinction, quartz granules subrounded. Five% of algae and foraminifera are tested with a micritic wall and are filled internally with microscopic grains. Porosity is greatly reduced due to their filling with depressed dwarfs. The new form is observed to worsen from micrite to microspar. The evaluation of thin sections allows the analysis of pore structure and

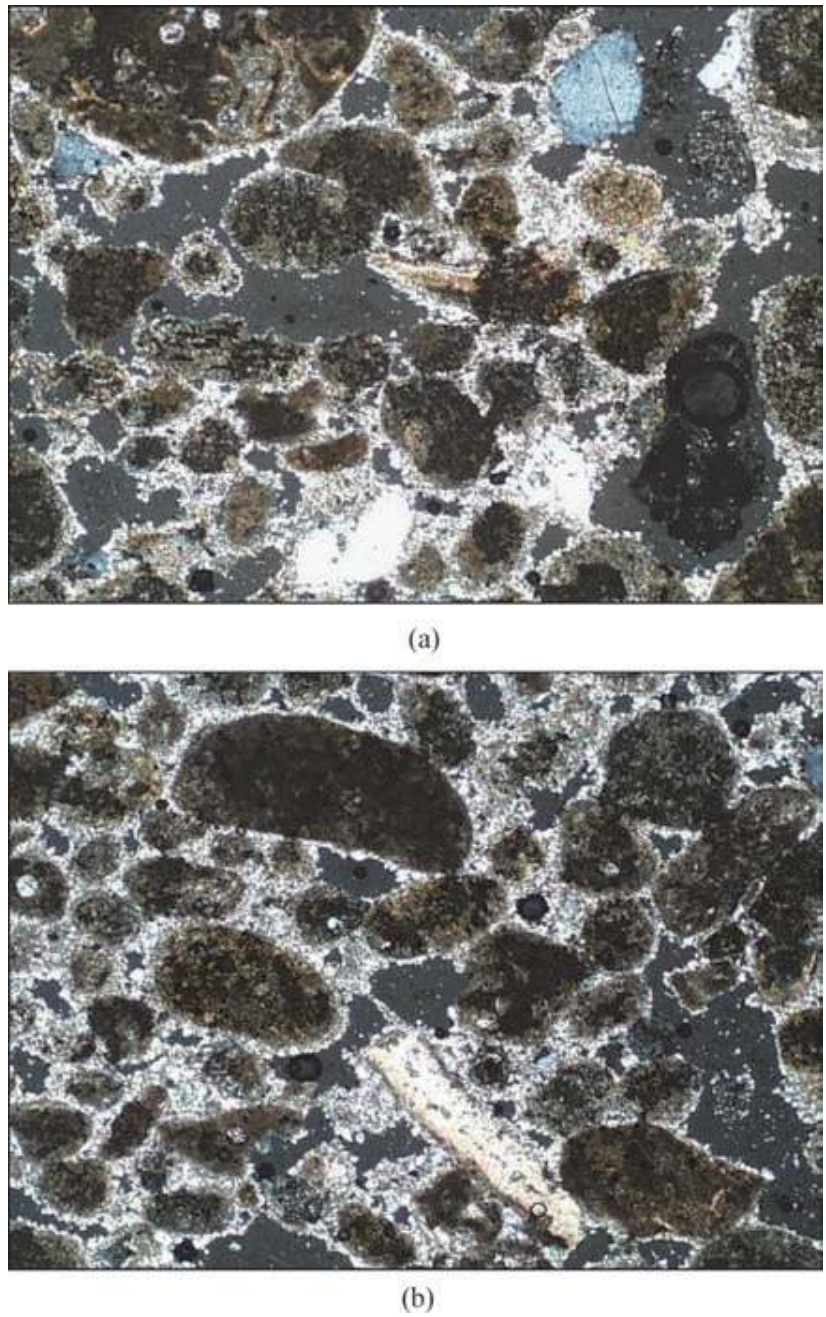

Figure 4.
(a, b) Photomicrograph of intact calcarenite under cross polarized light (XPL) showing wackestone (pele-oosparite) texture with drusy sparite, Mustafa Kamel Necropolis (Weathered sample, heterogeneous pore system).

enables the assessment of pore size and distribution in relation to the distribution and formation of the minerals involved.

4.4 Comparison between the sound and weathered rock layers

Samples can be clearly distinguished from the alveolar portions - the amortized and non-woven parts using thin, unpainted limestone sections that feature a relatively homogeneous pore structure. In contrast to unpainted areas, alveolar flats have a heterogeneous pore structure, for example pores often contain ferric oxides and hydroxides indicating a lower total pore size and higher content of small spots.

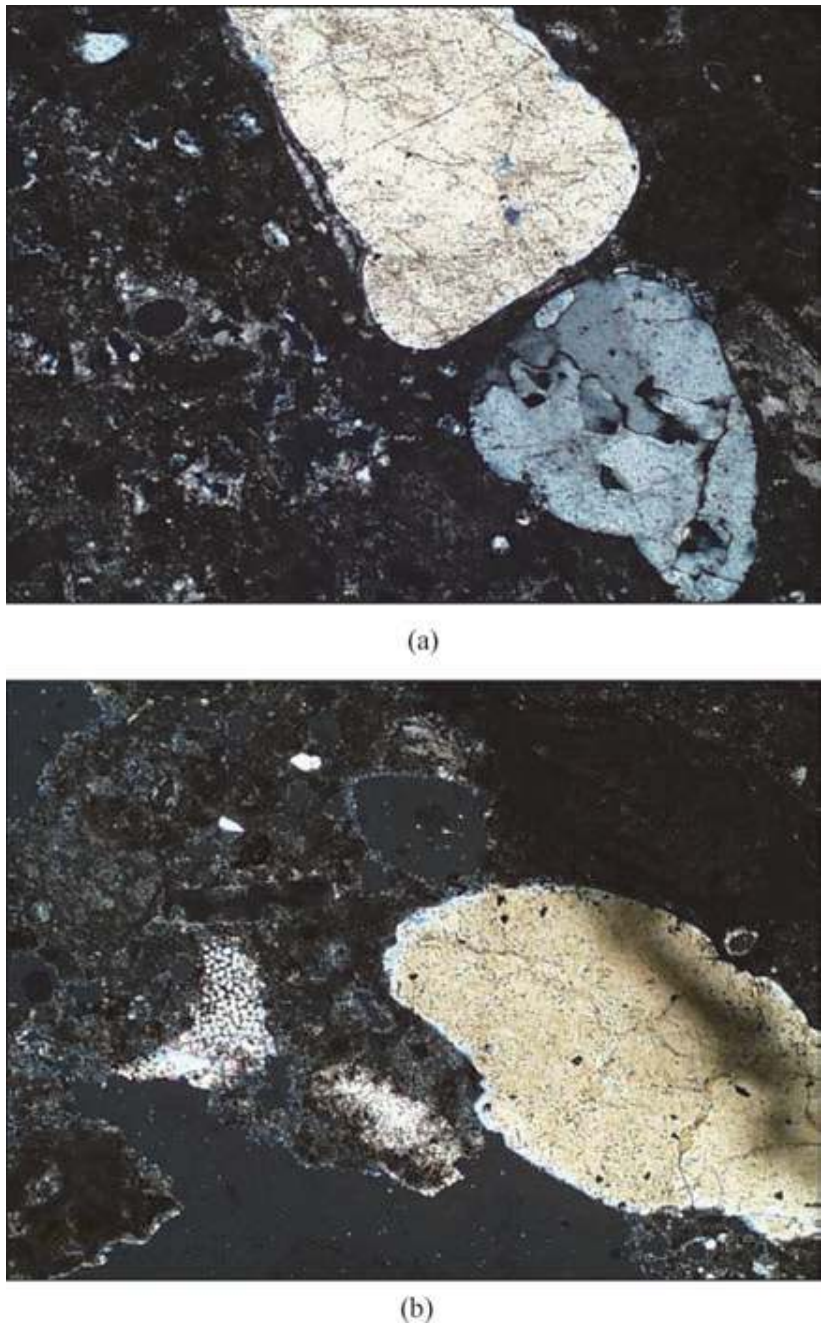

Figure 5.
(a, b) Photomicrograph of fossiliferous oolitic intraclastic limestone thin section under cross-polarized light (XPL) showing subrounded monocrystalline quartz grains (QTZ) and porous region, El-Shatby Necropolis.

Data from microscopic polarization and electron microscopy experiments show that oxygen clarity of NaCl crystals is strongly influenced by the rate and volume of moisture changes, and how they shrink with changes in crystal size.

5. Creep tests (materials and experimental program)

Creep is an irreversible ductile deformation in time under constant stress. Creep strain seldom can be recovered fully when the loads are removed, thus it is largely

"plastic deformation." It is a progressive phenomenon initiated at a certain time after excavation at a certain location around the profile and spreading in time into the rock mass. For the long-duration design life of underground structures, the long-term stability of the tunnel must receive major consideration. For this reason, time-dependent deformation behavior of the surrounding rock must be well understood. Neglecting creep effects during deep excavation may lead to incorrect evaluation of deformation and thus may impact on the criteria for selection of proper design.

Understanding the mechanisms of rock breakdown that have been excavated within ancient monuments requires a thorough study of the mechanical behavior of these rocks, and the importance of the physical and mechanical properties of these rocks to understand the phenomena of instability.

The results of the geotechnical characterization of these rocks will be used in numerical modeling and design of reinforcement measures. For this purpose, a new laboratory testing program will be launched.

Rocks, sample preparation, experimental setup used and the procedure are briefly described below.

5.1 Types of creep

An idealized creep curve for rock at constant stress consists of three stages: instantaneous elastic strain followed by primary creep with decreasing creep rate, then steady-state creep with constant creep rate, and finally tertiary creep with increasing creep rate leading to failure. Most of the work on time-dependent strain has been conducted on primary and secondary creep phases only and the tertiary phase has not been investigated in appreciable detail.

5.2 Laboratory test specimens

In this study, the size of the comprehensive laboratory testing program using cylindrical samples with 42-44 mm diameter and height (91–103 mm). Although these rocks do not show distinct layers, the nuclei were extracted from the blocks and their masses in the vertical direction, which was expected to represent the physical properties of these units perpendicular to the layers. However, some samples were also extracted in a vertical direction on the mattress. Some specimens were broken and/or small cracks or cracks appeared on their surfaces. However, in order to achieve reliable assessments, the number of samples was increased as many as possible. Laboratory tests were performed in accordance with the testing procedures proposed ISRM and recommended by ASTM at the Engineering Geology Laboratory, Department of Civil Engineering, University of Aristotle Thessaloniki, Greece.

5.3 Laboratory tests

Laboratory studies (experimental examination) were performed on surface rock samples and prepared surfaces. The basic mechanical testing of the laboratory includes the behavior of deformation to failure under uniaxial and triaxial compression and we offer a complete creeping rock characterization conducted during the past 2 years from a series of isotropic and isotropic compression tests conducted in the inventory of various stresses, viscosity behavior was determined by following a procedure, the multi-step download, which emphasizes the transit creep side.

5.4 Very slow uniaxial creep tests on calcarenitic and sandy oolitic rock specimens under investigation

Creep in hard brittle rocks is rare as deformation rate is extremely slow. Hard rock shows creep behavior appreciably only at elevated temperatures and pressures generally not encountered in engineering structures. Soft rocks on the other hand creep mostly at the room temperature, atmospheric pressure, and deviatoric stress range normally encountered in engineering structures.

5.5 Analysis of creep behavior of soft rocks in tunneling

Regarding viscous plasticity, despite much work done on high porous rocks, only over the past years, there has been growing concern about the long-term behavior of deep underground structures in general. The rock mass tests large strain rates of viscosity and plastic. However, after a few years, the stress rates become smaller and reach a fairly stable condition characterized by very small stress rates.

It is known that most rocks have time-dependent behavior, and the viscous and plastic modeling of rocks and soils is of great importance both in petroleum engineering and underground engineering, for example when assessing deformations at the walls of deep fossil sections or considering pressure problems.

Moreover, when smaller time periods are considered, the stress distribution around a cave or exposures is such that the divergent pressure decreases rapidly with respect to the distance to the cave. Very small stress rates are tested at large distances within the rock mass and should be evaluated when predicting the behavior of the cave or photo gallery [40].

The limited available literature may be rooted in the particular problems raised by the long-term creep test, in the short term, as described below.

1. When the creep rate is $10 = 10^{-12}\ s^{-1}$, a 12-day test results in a strain of $\varepsilon = 10^{-6}$. The coefficient of thermal expansion of rocks is in order $\alpha = 1^{-4} \times 10^{-5}\ C^{-1}$, that is, the "noise" (i.e., elastic thermal deformation sample) due to small temperature changes will be greater, in most cases, than the signal to be measured (e.g., the average sample deformation arose from proper creep). The same can be said for moisture variations, which have a significant impact on many rocks.

2. Slow creep rates are obtained when small mechanical loads are applied. Most of the crawl test devices are designed to work in a DVR pressure range of 5–20 MPa. Stress control is usually weak when the applied pressure is less than 1 MPa.

3. The creep rate is calculated by comparing strains $\varepsilon_{1,}$ measured in two different times, τ_1 and $\tau_{2,}$ or $\varepsilon. = (\varepsilon_2 - \varepsilon_1) / (\tau_2 - \tau_1)$. When the compression rate is in the range $\varepsilon = 10^{-12}\ s^{-1}$, it can be reasonably evaluated on a daily basis ($t_2 - t_1 = 105$ s, $\varepsilon_2 - \varepsilon_1 = 10^{-7}$) only if ε_1 and ε_2 can be measured with an accuracy of not less than 10.8, or one-tenth of the expected difference between the two successive measured breeds [40].

Tightening of fragile rocks results in distributed damage long before the rocks fail unstable. The damage is usually manifested in small fractures and expansive microcracks [41–43]. These small fractions are usually smaller than the grain size and are often distributed almost uniformly before they are locally cracked. There are no uniform distributions of small fractions associated with the nucleus of error and growth.

Partial damage was used to explain the reduction of seismic wave velocity, earthquake variation, reduction of elasticity and strength units, and rock failure mechanics. In addition, stress damage can facilitate time-based creep-driven by stress erosion and subcritical crack growth. This creep strongly affects long-term strength and failure stability. For example, granite samples that are exposed to 1 month of non-axial static pressure under a pressure of approximately 0.65 may fail—or "delayed fractures" may develop days to years after removal of applicable loads.

The creep test shows how strain builds up over time under constant pressure. The rock usually deforms quickly and then begins to deform more slowly after the yield fatigue, which is called the initial creep. After the initial creep (I), the deformation continues at a constant rate in the linear part of the curve, which is secondary creep (II). Finally, the deformation rate increases rapidly until the rock fails to "fracture" in the high creep (III), if stress is removed but the strain remains permanent.

Three stages of creep behavior can be identified: in the first stage, they are classified as initial creep, and strain occurs at a decreasing rate. In some cases, the primary creep curve approaches a constant rate of strain called secondary creep. In high-stress specimens, secondary creep may turn up in higher creep, which is characterized by an increased strain rate until creep failure occurs suddenly. In the last two stages, the thin vertical cracking begins, accompanied by hardening, and only near failure, large cracks spread rapidly and lead to a sudden collapse. Long-term tests performed on a secondary creep sample revealed even appearance at 40% of estimated strength. The purpose of this research is to make recommendations on the promotion and safety of long-term underground historical structures under load. For this purpose, there is a set of experimental tests and advanced numerical analyses.

6. Description and discussion of the experimental program

6.1 Describe full creep tests

The research demonstrates an integrated empirical approach aimed at assessing safety and strengthening historic underground structures under high pressure.

The purpose of these tests is to obtain data, first, to determine the amount of sticky parameters that govern the long-term behavior of these structures, and secondly, to validate numerical models.

6.2 Testing device

Long-range uniaxial creep tests were performed on standard cylindrical rock samples collected from the three archeological sites under investigation (diameter D = 4.2–4.4 mm, height H = 90–103 mm); samples were prepared for testing according to ASTM standards with length-to-diameter ratios approximately 2.25, all samples have highly polished end surfaces to minimize final effects. The sample was set between two solid steel plates, with a steel cover between the sample and the two plates. During each test, two high-precision displacement sensors at two vertical levels at a 90° angle allowed both the relative rotation of the two pages and the measurement of the average relative displacement.

6.3 Sensors

Applied loads and the resulting strain were recorded using an automatic data acquisition system, sampling at a rate between 1 and 3 readings per second, thereby overcoming any deficiencies in data resolution.

6.4 Loading

The approved test procedure consisted of loading samples at a constant rate of about 1.35 MPa up to 1.75 MPa for samples from Catacomb in Kom El-Shoqafa, 1.55 MPa up to 2.17 MPa for samples from Mustafa Kamel Necropolis, and 2.6 MPa up to 3.44 MPa for samples from El-Shatby cemetery. In order to keep the applied pressure as stable as possible, dead weights were used and steel cylinders were placed on the upper steel plate on the upper face of the cylindrical sample. The applied stress is calculated by dividing the weight of the steel cylinders placed on the top plate by the initial cross-sectional area of the sample.

6.5 Temperature and hygrometry

The temperature changes during a long-term creep test must be as a small as possible and must be measured precisely enough to allow correction of the raw strain data for thermoelastic strains; in our study, all the periods of test were in the room temperature between 24 and 26° in the laboratory by controlling the air condition.

7. Test results

Uniaxial creep tests were performed on three rock samples from each site. Rock samples are loaded through fixed uniaxial compression at 1, 35, 1, and 75 MPa (one stress per sample) for Catacomb of Kom El-Shoqafa rock samples collected, at 2.6 and 3.44 MPa for rock samples collected from El-Shatby archeological site, and at 1.55 and 2.17 MPa for rock samples collected from Mustafa Kamel Necropolis.

The experimental procedure follows ASTM standards (ASTM D4405 and D4341). The compression machine is used to apply continuous axial load to the samples. Digital scales are installed at 0.001 millimeters to measure the axial displacement of the samples, see **Figures 6–9**. Samples are loaded continuously for 1 to 2 years until the samples fail without any acceleration, depending on the displacement results. During testing, axial distortion, time, and failure modes are recorded. The readings are repeated every minute at the beginning of the test, and gradually decrease to twice a day after the first few days of testing. This also depends on the deformation rate of each sample. The results are presented by strain time curves. Axial stress and axial pressure values are calculated by:

$$\sigma_{\text{axial}} = \text{Pa}/\text{A}, \tag{1}$$

$$\varepsilon_{\text{axial}} = \Delta\text{L}/\text{L}, \tag{2}$$

where σ axial is the axial pressure, Pa is applied axial load, A is the normal cross-section area of the direction of the load, $\varepsilon_{\text{axial}}$ is the geometric axial strain, ΔL is the axial deformation, and L is the original length.

Table 2 summarizes the results of a uniaxial creep test. The axial stress time curves are shown in **Figures 10–16**, and the curves represent instantaneous, transient, and triple creeps of rock samples under a fixed axial load. Samples are loaded quickly and then the axial strains increase. The immediate breeds range from 0.07 to 3.5.

Most samples, under constant axial pressure, show a complete creep stage: transient, steady, and triple creep stages.

Increasing the value of the instantaneous creep strain with hard axial stress gives strain time curves of rock samples tested under constant high and low axial

Figure 6.
Rock creep testing devices. Samples are 90–105 mm high, 42–44 mm² diameters. Two displacement sensors were used during each test.

Figure 7.
The collected intact sandy oolitic limestone specimens from El-Shatby Necropolis site under creep testing devices.

pressures. Axial stress also increases crawling strains. In the transit crawl stage, the stress rate increases with the applied stressors. In most cases, the stress rate under high axial pressure is greater than the low axial pressure rate. The effect of embedding in the sample may make the compression rate under low pressure higher than the pressure under high pressure.

7.1 Catacomb of Kom El-Shoqafa, Test No. 1

On May 5, 2016 (Day 1), Catacomb of Kom El-Shoqafa no_1 began testing on a sample of sandy limestone, loading it to a vertical stress of σ1 = 1.75 MPa, 65% of the coaxial compression strength of the rock material (peak sample strength). **Figure 10** displays the strain curve versus time; this curve averages the data provided by two displacement sensors. Strains do not correct for elastic thermal differences. In this test, the crawl was faster than the Catacomb of Kom El-Shoqafa site. Test no_2: From day 130 to day 200 after the start of each test, the cumulative strain was 4.5

Figure 8.
The collected sandy oolitic limestone specimens from the catacombs of Kom El-Shoqafa site under creep testing devices.

Figure 9.
The collected intact calcarenitic rock specimens from Mustafa Kamel Necropolis site under creep testing devices.

microns for Catacomb of Kom El-Shoqafa. 1 and 2.8 microns for Catacomb of Kom El-Shoqafa test site 2. This difference is fully in line with what is known in previous tests conducted at greater pressures on these samples. When the stress rate in the transient pressure zone is increased, followed by a similar decrease, it can be observed from day 44 to day 130, immediately followed by a steady slope (steady state crawl) up to 205 days. Finally, a more stable condition followed with a smaller stress rate until the sudden sample failure on day 368. Stress rate developments were more progressive in this case. There is no specific explanation for these changes in compression rate. At the end of the test, the observed pressure rate is $\varepsilon = 2.30 \times 10^{-8}\,s^{-1}$, the sample was suddenly broken after the 368 day (end of the test) on June 1, 2017, while the sample showed a higher creep phase.

7.2 Catacomb of Kom El-Shoqafa, Test No. 2

On September 1, 2016, (Day 1) after the start of the previous tests, an identical creep device on the same table was assigned to the catacomb of Kom El-Shoqafa

Specimen No.	Testing period	Time (days)
		1 9 100 135 178 375 667 786 813
Catacomb of Kom El-Shoqafa test N_1 (sandy oolitic limestone)	From **5/5/2016** to **1/6/2017**	**σ_1 = 1.35 MPa**
Catacomb of Kom El-Shoqafa test N_2	From **1/9/2016** to **2/7/2018**	**σ_1 = 1.75 MPa**
El-Shatby Necropolis. test N_1 (oolitic intraclastic limestone)	From **12/4/2016** to **4/7/2018**	**σ_1 = 2.60 MPa**
El-Shatby Necropolis. test N_2 (oolitic intraclastic limestone)	From **5/5/2016** to **3/7/2018**	**σ_1 = 3.44 MPa**
Mustafa Kamel Necropolis .test N_1 (intact Calcarenite)	From **3/4/2016** to **22/3/2017**	**σ_1 = 1.55 MPa** **σ_1 = 1.86 MPa**
Mustafa Kamel Necropolis. test N_2 (intact Calcarenite)	From **11/4/2016** to **28/3/2017**	**σ_1 = 2 MPa**
Mustafa Kamel Necropolis. test N_3 (intact Calcarenite)	From **6/4/2016** to **7/4/2016**	**σ_1 = 2.50 MPa**

Table 2.
Uniaxial creep test, testing program.

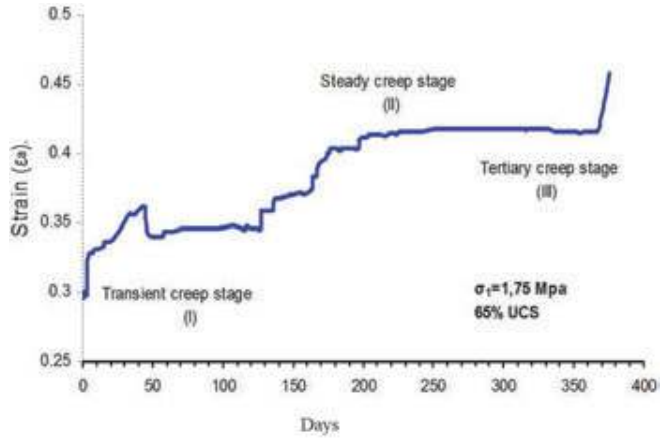

Figure 10.
Strain versus time curve during the catacomb of Kom El-Shoqafa, uniaxial creep test no. 1.

Test no_2, which began on another sample significantly purer than the previous, loaded on a vertical stress σ1 = 1.35 Mpa, 50% of the axial compression strength of the rock material (peak strength), the applied stress until the end of the test was not adjusted without sample failure on July 2, 2018, during a steady slope or steady state and a creep with a small strain rate was observed. **Figure 11** displays a curve versus time. This curve averages the data provided by two displacement sensors. The compression rate (ε.) is calculated every 5 days; it is calculated for 10 days. Strains are corrected for temperature variation. Initially, the strain experienced a long initial transient period until the first few days characterized by a slow decline in rate, with the average stress rate stabilizing to $\varepsilon = 5.85 \times 10^{-10}\ s^{-1}$ (positive sample contractions), with long-term amplitude fluctuations ++20%; this is probably associated with moisture fluctuations. This phase was followed by a long steady slope or steady-state creep to the end of the test while the observed compression rate was ε. $= 3.21 \times 10^{-9}\ s^{-1}$, while it was $1.50 \times 10^{-9}\ s^{-1}$ was at the beginning of the test.

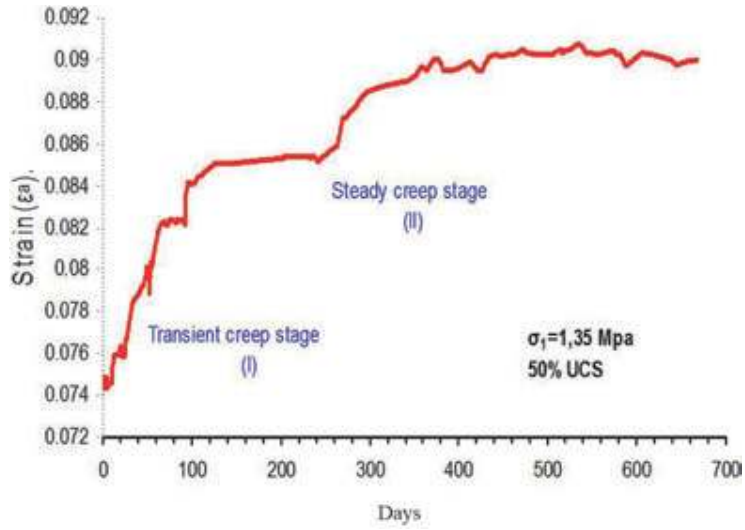

Figure 11.
Strain versus time curve during the catacomb of Kom El-Shoqafa, uniaxial creep test no. 2.

7.3 El-Shatby Necropolis, Test No. 1

On April 12, 2016, (Day 1) testing of Shatby Tombs No. 1 began on a sample of sound rock-limestone that was loaded to = 1 = 2.60 MPa, 50% of the axial compression strength of the rock material (peak strength) is not Stress adjustment until the end of the test on July 4, 2018. **Figure 12** shows the stress curve versus time, where the elastic strain is followed by a long transient creep characterized by a slow rate of decline, followed by a slope or creep constant in a steady state with a small stress rate until end of the test without sample failure; this curve averages the data provided by two displacement sensors. The compression rate (ε.) is calculated every 1 h at the beginning of the test, and after the first few days it is calculated every day. Strains are corrected for temperature variation. The strain experienced a long initial transient period, where the average stress rate stabilized on $\varepsilon = 1.3 \times 10^{-9}\ s^{-1}$ (positive sample contractions.), with long-term amplitude fluctuations ++15%; this is probably associated with moisture fluctuations.

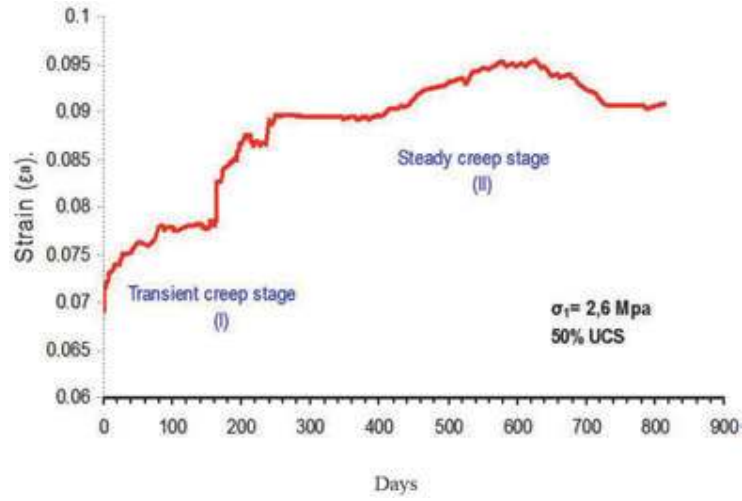

Figure 12.
Strain versus time during El-Shatby Necropolis, uniaxial creep test no. 1.

Transient reverse crawl was observed on day 214 to day 244, sometimes referred to as "hypotension." During this test, this reverse crawl lasted much longer (20 days) than is currently observed in tests with greater stress. The stress rate stabilized one way or another after day 260, but at the end of the test, the observed pressure rate was $\varepsilon. = 1.62 \times 10^{-9}\ s^{-1}$.

7.4 El-Shatby Necropolis, Test No. 2

On May 5, 2016 (after the start of the previous tests), an identical crawl device was assigned to the same table, and El-Shatby test of Q2 was started on a cylindrical sample with geometric dimensions similar to that used in El-Shatby test of cemetery no_1, loaded on a vertical stress of σ1 = 3.44 MPa, 65% of the coaxial compression strength of the rock material (**Figure 13**). A long transient period can be observed followed by a constant inclination or a steady-state crawl until the last day of recording. In this test, the crawl was faster than at El-Shatby Cemetery, test number 1: from day 70 to 270 after the beginning of each test, the cumulative strain was 2.5 μm for El-Shatby Cemetery, test number 2 and 1.8 microns for El-Shatby Cemetery site, test number 1. This difference corresponds exactly to what is known from previous tests conducted at greater pressures on these samples. An increase in the stress rate can be observed, followed by an equivalent decrease, at day 260 and at around day 324, and stress rate developments were more progressive in this case. There is no specific explanation for these changes in compression rate. At the end of the test on July 3, 2018, the observed pressure rate was $\varepsilon. = 3.41 \times 10^{-10}\ s^{-1}$.

7.5 Necropolis of Mustafa Kamel, Test No. 1

On April 3, 2016, (Day 1) Mustafa Kamel's # 1 test began on an intact sample initially loaded at 1.55 MPa but no creep was observed until 9 days after the test began. Perhaps the pregnancy is too small to produce any detectable strain. Thereafter, the applied pressure was adjusted once, and was constructed up to σ1 = 1.86 MPa (+10%) after the 9th day 60% of the uniaxial compression strength of the rock material. The numbers in parentheses indicate that the compression value is adjusted. **Figure 14** shows the pressure curve versus time; this curve averages the data provided by two displacement sensors. The compression rate (ε.) is calculated

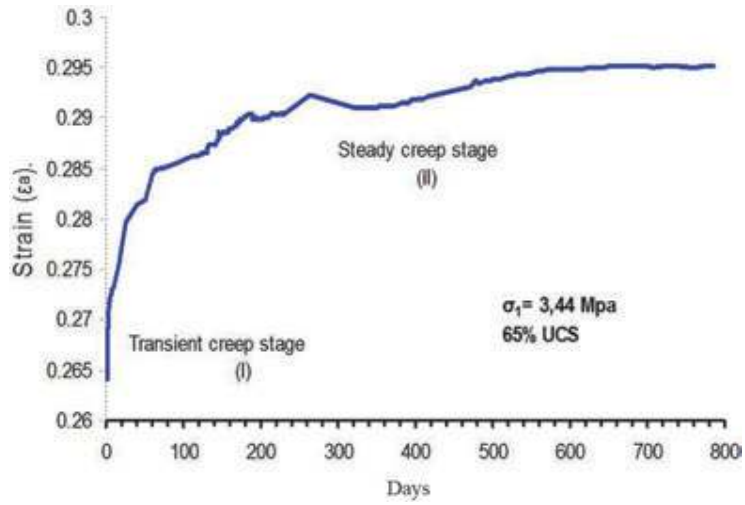

Figure 13.
Strain versus time curve during El-Shatby Necropolis, uniaxial creep test no. 2.

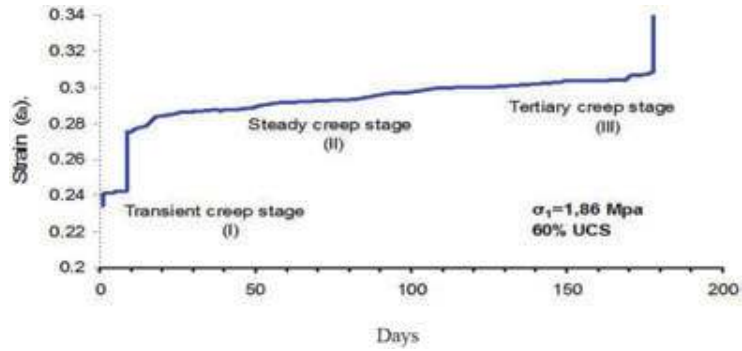

Figure 14.
Strain versus time curve during Mustafa Kamel Necropolis, uniaxial creep test no. 1.

every 5 days; it is calculated for 10 days. Strains are corrected for temperature variation. The strain experienced a long initial transient period characterized by a low slow rate followed by a steady slope or a steady-state creep with a small stress rate, at which time the average stress rate stabilized to $\varepsilon = 1.62 \times 10^{-9}\ s^{-1}$ (positive sample contractions.), with long-term capacity fluctuations of + _20%; this is probably associated with moisture fluctuations.

The transient inverse creep has not been observed, and is sometimes referred to as "stress drop." Strain rate more-or-less stabilized after day 160, and strain rate $\dot{\varepsilon} = 4.86 \times 10^{-9}\ s^{-1}$ and the sample has been broken suddenly after 178 days (the end of the test 22/3/2017); the specimen showed the complete three phases of creep end with the tertiary or acceleration creep stage.

7.6 Necropolis of Mustafa Kamel, Test No. 2

On April 11, 2016, (after the start of the previous tests) an identical crawl device was set on the same table, and Mustafa KAM # 2 test started on another sample that is significantly purer than the previous, loaded on the stress of σ1 = 2 MPa, 65% of the uniaxial compression force for rocky materials, and applied pressure was not modified until the end of the test on 28/3/2017 (**Figure 15**). It displays the strain curve versus time; this curve averages the data provided by two displacement sensors. In this test, the creep was faster than the site of Mustafa Kamel's tombs, test number 1: from day 11 to 91 after the start of each test, the cumulative strain was 3.7 microns for the Mustafa Kamel test site Necropolis. 2 and 3.5 microns of the graves of Mustafa Kamel site No. 1. This difference corresponds exactly to what is known from previous tests conducted at greater pressures on these samples. An increase in

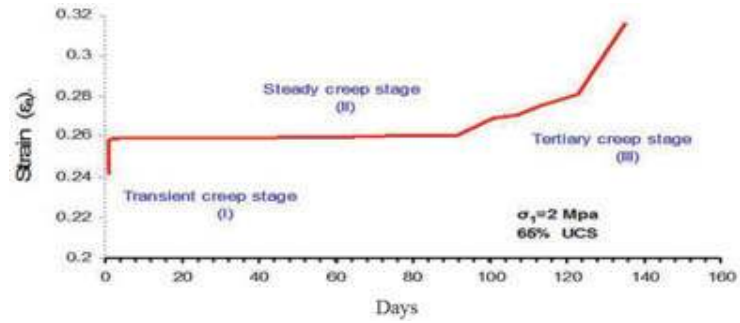

Figure 15.
Strain versus time curve during Mustafa Kamel Necropolis, uniaxial creep test no. 2.

stress rate was not observed in this test, followed by an equivalent decrease, while a long transient strain was encountered and a slow decline in rates was followed by a creeping phase in a steady state with a very small stress rate until day 91, after acceleration or the third stage of creep began. The 135th day in a large stress rate $\varepsilon. = 1.11 \times 10^{-9}\ s^{-1}$.

7.7 Necropolis of Mustafa Kamel, Test No. 3

On April 6, 2016, an identical creep device was set on the same table, and Mustafa KAM # 3 test was started on another heavily loaded sample on a stress of σ1 = 2.5 MPa, 80% of the uniaxial pressure force of the material rock (peak strength). Strains do not correct for elastic thermal differences. **Figure 16** displays a curve versus time. This curve averages the data provided by two displacement sensors. In this test, the crawl was faster than the site of Mustafa Kamel's tombs, test number 1 and test number: from the first day after the start of the test, the cumulative strain was 7 microns for the site of Mustafa Kamel Necropolis, test number 3. This difference corresponds exactly to what is known from the tests previously conducted at smaller pressures on these samples. The sample fractured 26 h after the start of the test, the crawl begins with a short elastic strain followed by a short transient strain followed by a steady-state crawl with a very small stress rate up to 23 h after the start of acceleration or triple crawl resulting in a sudden failure of the sample with a high stress rate after 26 h exactly. At the end of the test, the observed pressure rate was $\varepsilon. = 0.30$ per second.

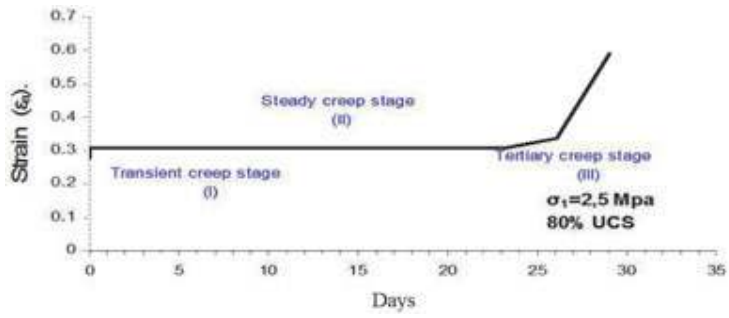

Figure 16.
Strain versus time curve during Mustafa Kamel Necropolis, uniaxial creep test no. 3.

7.8 Comparison with tests performed under larger stresses

Qualitatively, the behavior of soft rocks under small pressure (0.1 = 0.1–3 MPa) exhibits the same general features as observed under large pressures (e.g., σ = 5–20 MPa). The rapid accumulation of stress leads to a transient creep characterized by a slow rate of decline. The creep rate then becomes almost constant (a steady state is reached) or, more precisely, its average value remains constant, but the rate faces long-term fluctuations that may be affected by slow changes in moisture measurement. Reducing the load ("low pressure") creates an inverse crawl, which lasts much longer during tests under greater stress.

Norton-Hoff's constitutive equation is often proposed to describe stable state creep.

$$\varepsilon^{\cdot} = A^{*} \exp.(-Q/RT)\, \sigma^{n} \qquad (3)$$

where σ is the applied deviatoric stress; T is the absolute temperature; and A*, n, and Q/R are constants. For Etrez salt, Pouya suggests the following parameter values:

$$A^* = 0.64\ \text{MPa}^{-n}\ \text{yr.}^{-1},\ Q/R = 4100\ \text{K, and } n = 3.1. \quad (4)$$

Berest et al. [40] found that if the Norton-Hoff Law of Conditions was derived in Creep Test 1 (σ = 0.108 MPa, T = 286.5 K), the calculated compression rate ($\varepsilon. = 10^{-17}\ s^{-1}$) is smaller. Start by from the observed compression rate ($\varepsilon. = 1.4 \times 10^{-12}\ s^{-1}$). The observed pressure rates, even if they are too small, are much larger than expected. Spears et al. suggest that the pressure solution (rather than infiltration and slip, the mechanism that controls high stresses) is the most effective mechanism for crawling at very small pressures; the exponent of stress in this context would be n = 1 instead of n = 3–5, which is observed during standard tests. If this proposal is adopted, the Creep law should be modified when considering small pressures, with significant consequences in predicting the cave or gallery convergence rate.

Many lessons were learned during the test under these unusually low pressures. This first series of tests opened the way for further research on the behavior of rocks under very small pressures, long-term single-axis crawl tests were performed for geological and engineering applications on rock samples (for 850 days), and the applied loads were as small as 1.35 MPa. Slow stress rates such as $1.11 \times 10^{-10}\ s^{-1}$ were observed in some cases. These small loads and pressure rates pose several specific problems: potential drift of sensors during long 2-year tests, interference with small changes in room temperature and moisture measurement, and effects related to irregular load distribution applied to sample surfaces. These difficulties have been recognized and at least partially addressed. The qualitative results are in good agreement with what is known as the behavior of soft rocks under greater pressure; however, the observed pressure rates, even if they are extremely small, were much greater than expected.

The initiation, accumulation, and growth of cracks caused by stress in rocks are generally referred to as rock damage. Referring to the pressure caused by the crack is the load at which the sample will eventually fail, under prolonged loading, which they propose correspond to about 70–80% of the peak strength of the sample. It is also believed that the damage to the crack damage or the crack damage threshold point corresponds to the point at which the stress reflection or sample expansion begins. Corresponding to the volumetric stress gradient is approximately 70% of the estimated unrestricted compressive strength of the rock.

These stresses are well above the stress threshold for damage. It has been suggested that sample composition for unrestricted compression force tests reduces the spread of cracks. Many researchers suggest that the strain of the ring is generated between a stretch crack and the outer surface of a cylindrical sample. This breed may generate a confinement collar that limits the growth of continuous cracks.

Preliminary test results suggest that an alternative mechanism may affect the spread of unstable cracks. Under pure uniaxial loading conditions, a split can be expected parallel to the maximum pressure direction. The failure may ultimately be at the microscopic level due to the curvature of the rock slabs resulting from tensile fractures directed toward the maximum compressive pressure, as shown in **Figure 17**.

7.9 Triaxial creep tests on the calcarenitic and sandy oolitic rock specimens under investigation

The purpose of triaxial creep tests is to determine the viscosity and plastic parameters of the soft rock samples under confined conditions and to investigate

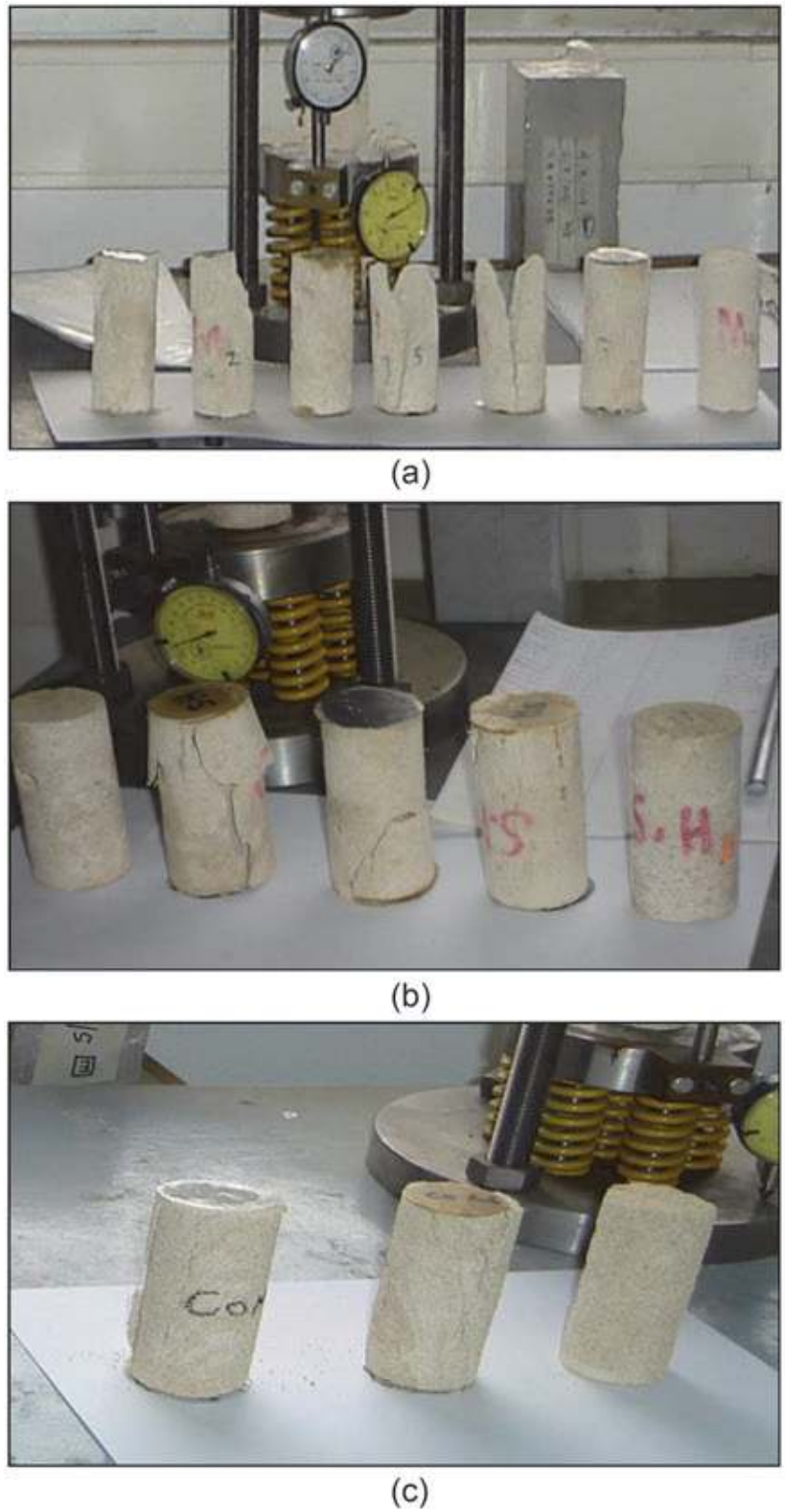

Figure 17.
Rock specimens under investigation, after uniaxial creep test. (a) Calcarenitic rock specimens, Necropolis of Mustafa Kamel. (b) Oolitic intraclastic limestone specimens, El-Shatby Necropolis. (c) Sandy oolitic limestone specimens, Catacombs of Kom El-Shoqafa.

the effects of axial stress and fortified pressure. Time-related parameters are monitored, recorded, and analyzed.

7.10 Test methods

Two samples of rock (length = 91–103 mm, diameter = 41–44 mm) were tested from each site under different constant axial pressures and different static pressure pressures for approximately 300 h. The experimental procedure follows the ASTM standard (ASTM D4406-93). The compression machine (fusion machine, 5000 kN) is used to apply the fixed axial load to the samples. Rock samples were placed in a three-axis cell (GDS) to provide constant confining pressure (**Figure 18**). The collected sample (Test # 1) of Catacomb of Kom El-Shoqafa is immediately loaded to the axial stress required at 1.45 MPa to limit the pressure by 225 kPa, and the applied axial stress was adjusted twice: the initial applied pressure was increased to 1 = 2, 17 MPa (+50%) after 98 h (2) then increased to σ1 = 2.53 MPa (+74%) after 125 h (3). The number in brackets refers to **Figure 18**, which displays the strain versus the time curve. Where the axial stress of up to 1.45 MPa and inventory pressures 510 kPa. Axial stress was not adjusted until the test ends after 200 h with steady-state creep with a small stress rate and without sample failure.

Figure 18.
Triaxial creep test device, with constant axial load under confining pressure. Triaxial creep test device. The cylindrical specimen placed inside (GDS) cell is loaded vertically using the compression machine.

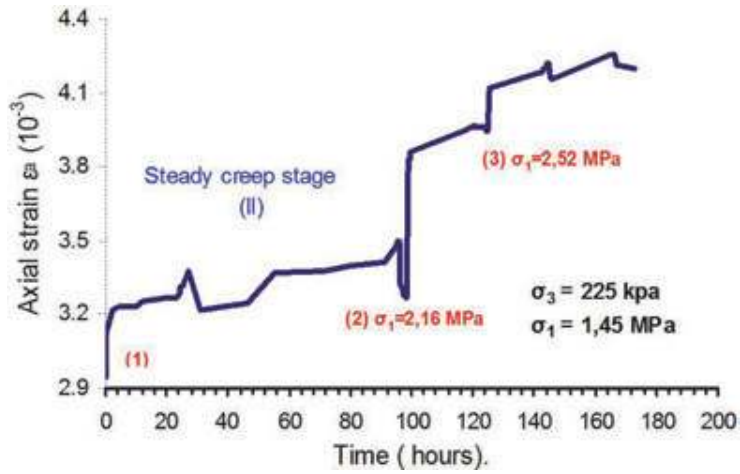

Figure 19.
Strain versus time during the catacomb of Kom El-Shoqafa, triaxial creep test no. 1.

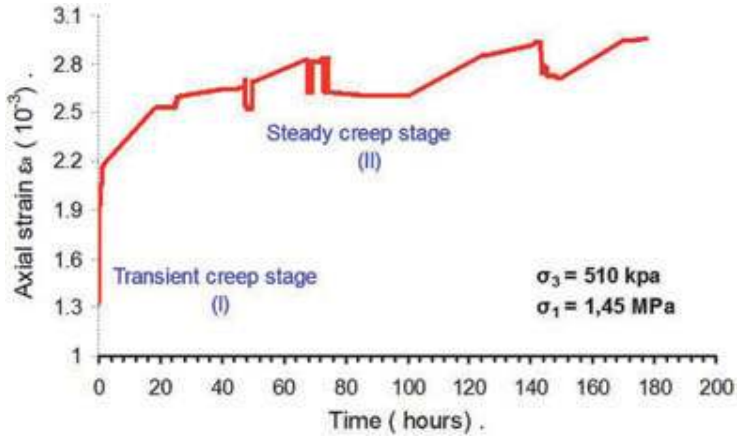

Figure 20.
Strain versus time during the catacomb of Kom El-Shoqafa, triaxial creep test no. 2.

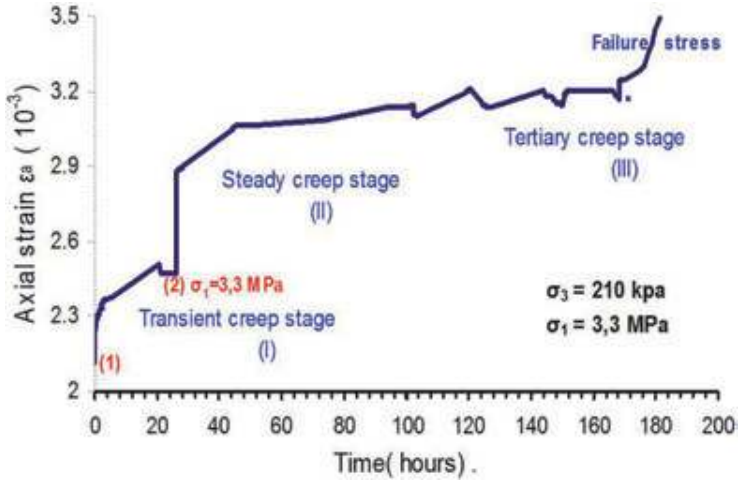

Figure 21.
Strain versus time curve during El-Shatby Necropolis, triaxial creep test no. 1.

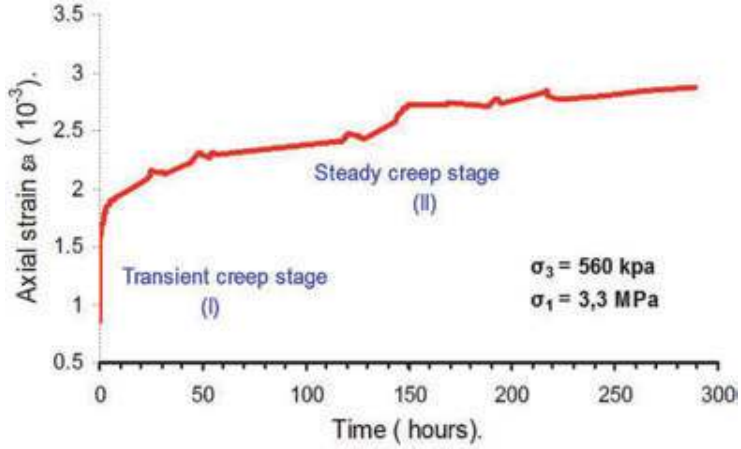

Figure 22.
Strain versus time during El-Shatby Necropolis, triaxial creep test no. 2.

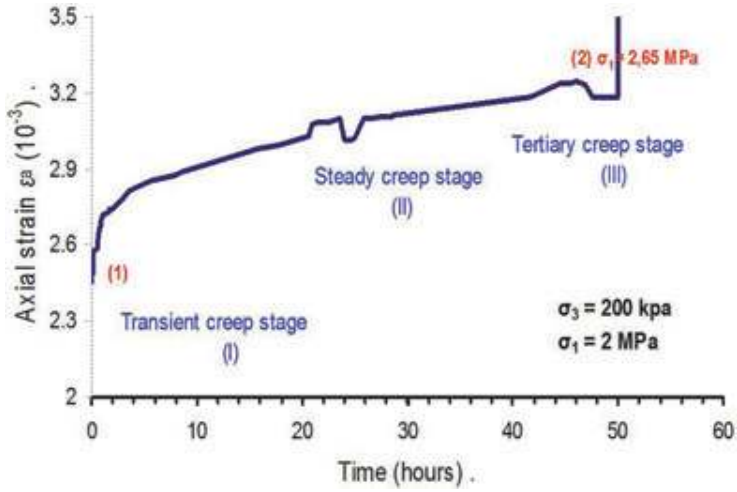

Figure 23.
Strain versus time during Mustafa Kamel Necropolis, triaxial creep test no. 1.

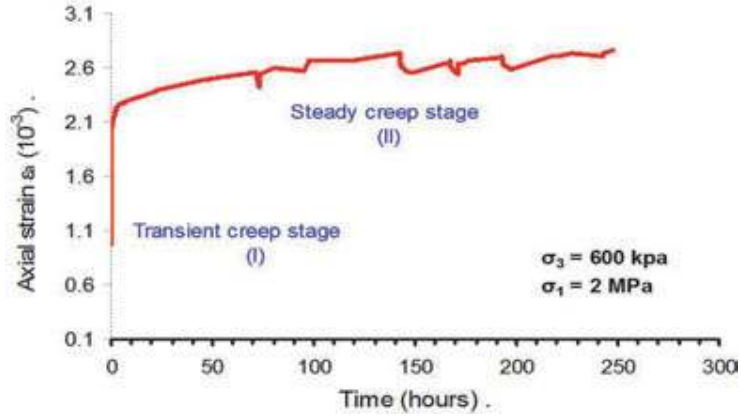

Figure 24.
Strain versus time curve during Mustafa Kamel Necropolis, triaxial creep test no. 2.

Samples collected (test # 1) from the Shatby Necropolis site were immediately loaded on the required axial stress at 2.63 MPa to limit pressure at 210 kPa, the applied axial stress was adjusted once: the initial applied pressure was increased to = 1 = 3.30 MPa (+25%) after 26 h (2).

In Mustafa Kamel Test No. 2, the sample was loaded on the axial stress required at 2 MPa to limit pressures of 600 kPa without modifying the axial stress until the end of the test at 300 h without high creep.

During testing, axial distortion and time are recorded. The frequency of reading is once every second at the beginning of the test, and gradually decreases to once every half an hour after the first day of the test. This also depends on the deformation rate of each sample. The results are presented by stress time curves in **Figures 19–24**. Axial stress and axial pressure values are calculated.

8. Test Results

8.1 Catacomb of Kom El-Shoqafa site

Axial strain time curves are shown in shapes (**Figures 19** and **20**). The curves represent transient and transient creep conditions of rock samples under constant

axial load and compression pressure. Instantaneous strains were observed immediately after loading the range from 3×10^{-3} to 3.2×10^{-3} for the test number_1, and 1.3×10^{-3} to 2.2×10^{-3} for the test number_2. All samples show a long "slow low" primary transient creep and steady-state creep stages until the end of the test without acceleration or triple creep resulting in sudden failure. Observations on subsequent tests show that deformation increases rapidly at first to the first few hours of testing and tends to remain constant after that. Stress rates in a steady state are 0.01 to 0.02×10^{-3} h^{-1}.

In this test, it was observed that crawling during the catacomb of Kom El-Shoqafa site Test no_1 (where = 3 = 225 kPa) was faster than crawling during the catacomb of Kom El-Shoqafa site test no_2 (where = 3 = 510 kPa) with the same axial pressure σ1 = 1.45 MPa: From 1 to 96 h after the start of each test, the axial strain accumulated (10–3) 3.5 for the catacomb of Kom El-Shoqafa site Test No. 1 and 2.7 for the catacomb of Kom Shoqafa website Test No. 2.

8.2 El-Shatby Necropolis

Axial strain time curves are shown in shapes (**Figures 21** and **22**). The curves represent temporary and transient creeps of rock samples under constant axial load and confined pressure. Instantaneous strains were observed immediately after the loading range from 2.5×10^{-3} to 2.9×10^{-3} for number_1 test, and from 0.91×10^{-3} to 1.8×10^{-3} for number_2 test. All samples show a long "slow low" primary transient creep and steady creep stages (constant slope) up to the end of the test at 300 h except test number_1, which showed acceleration or triple creep stage leading to a sudden sample failure at 180 h where the confined pressure σ3 was small, that is, 210 KPa, while at test number_2, it was 560 kPa and the axial pressure was the same for the eyes σ1 = 3.3 Mpa. Observations on subsequent tests showed deformation increases rapidly at first to the first few hours of testing and tends to remain constant after that. The first sample failed after the end of the test. Pressure rates in the steady state are 0.01 to 0.015×10^{-3} h^{-1}.

It was observed that creep through Shatby site Necropolis, test number 1 (where k3 = 210 kPa) was faster than creep through Shatby cemetery site, test no_2 (where = 3 = 560 kPa) under the same axial pressure σ1 = 3.3 MPa: From 1 to 150 h after the start of each test, the accumulated axial strain (10^{-3}) was 3.2 for Shatby Necropolis site Test site 1 and 2.4 for Shatby site Necropolis Test No. 2.

8.3 Mustafa Kamel Necropolis

Table 3 summarizes the results of the triple axial crawl test. Axial strain time curves are shown in shapes (**Figures 23** and **24**). The curves represent transient and transient creep conditions of rock samples under constant axial load and compression pressure. Strains observed immediately after the loading range from 2.5×10^{-3} to 2.7×10^{-3} for test number_1, and from 0.98×10^{-3} to 2.3×10^{-3} for test number 2. All samples show a long initial transient creep "characterized by slow rate of decline" and steady creep phases (constant slope) up to the end of the test at 300 h except the first sample, which shows a transient, steady, and triple-accelerated creep phase leading to sudden sample failure at 49 h immediately after adjusting the axial pressure from σ1 = 2 MPa to σ1 = 2.65 MPa. Observations on subsequent tests showed deformation increases rapidly at first to the first few hours of testing and tends to remain constant after that. Pressure rates in the steady state are 0.01 to 0.015×10^{-3} h^{-1}.

In this test, it was observed that crawling through the site of Mustafa Kamel's cemetery in test 1 (where = 3 = 200 kPa) was faster than crawling through the site of Mustafa Kamel's cemetery. No_2 test (where = 3 = 600 kPa) under the same axial

Specimen No.	Testing period	Confining pressure (σ_3)	Time (h)		
			1 3 26 51 52 98 125 200 300		
Catacomb of Kom El-Shoqafa test N_1 (Sandy oolitic limestone)	From **19/10/2016** to **27/10/2016**	**225 KPa**	σ_1 = **1.45 MPa**	σ_1 = **2.17 MPa**	σ_1 = **2.53 MPa**
Catacomb of Kom El-Shoqafa test N_2	From **21/11/2016** to **28/11/2016**	**510 KPa**	σ_1 = **1.4 MPa**		
El-Shatby Necropolis test N_1 (oolitic intraclastic limestone)	From **9/11/2016** to **16/11/2016**	**210 KPa**	σ_1 = **2.63 MPa**	σ_1 = **3.30 MPa**	
El-Shatby Necropolis test N_2 (oolitic intraclastic limestone)	From **29/11/2016** to **11/12/2016**	**560 KPa**	σ_1 = **3.31 MPa**		
Mustafa Kamel Necropolis test N_1 (Calcarenite rock)	From **16/10/2016** to **18/10/2016**	**200 KPa**	σ_1 = **1.32 MPa**	σ_1 = **1.98 MPa**	σ_1 = **2.6 MPa**
Mustafa Kamel Necropolis test N_2 (Calcarenite rock)	From **12/12/2016** to **22/12/2016**	**600 KPa**	σ_1 = **2 MPa**		

Table 3.
Triaxial creep test, testing program.

pressure = 1 = 2 MPa: from 1 to 45 h after the start of each test, the accumulated axial strain (10^{-3}) was 3.3 for Necropolis of Mustafa Kamel site Test no. 1 and 2.5 for the site of Mustafa Kamel cemetery test site 2.

Thus, the prevalence of cracking (in the fragile field) and pore breakdown (under high pressure conditions) are the prevailing deformation mechanisms of the selected rocks.

The cumulative results of various three-axis crawl tests, conducted at tight pressures ranging from 200 to 600 kPa, showed that crawling reduces the level of brittle stress on failure by 15–20% in relation to standard tests, and similarly, the resulting stress threshold (e.g., Pore breakdown (reduction)) is reduced by the same amount, while the volumetric component of the strain is diluted only in the absence of confined pressure, and shrinks completely even when σ3 decreases.

The instantaneous creep strain depends on axial pressure and confining pressure. In general, increased continuous axial pressure leads to greater axial stress. The pressure rate under high axial pressure is greater than the pressure under the lower axial pressure for the same fixed pressure. The higher the confined pressure, the smaller the resulting pressure. Comparison of results obtained from other soft rocks/salts indicates that the stress rate depends on the stress and previous strain. This is also consistent with the conclusion of Courthouse and Ong et al. who describe soft rocks as close.

The time-based foundational model of soft rocks developed by Zhang et al. can reproduce the general crawl characteristics of soft rocks with high precision. The crawl failure time to load the strain of the aircraft is longer than that of the three-axis load because the strain load frame controls the sample to expand.

9. Micromechanics of creep in the calcarenitic rocks

There is now a large body of evidence that rock deformation at low temperatures and pressures occurs through two mechanisms widely referred to as faulty flow and ductile flow. The term ductile is often used in three different contexts, including (1) plastic

deformation of single crystals, (2) homogeneous deformation or uniform flow, and (3) deformation over a certain amount of stress. Here we will use the term ductile in the macroscopic sense of homogeneous deformation where inferior microscopic processes include improved shear pressure, granulation, and granular flow.

Macroscopically, these microscopic processes form the flow of the calcite. Experimental evidence of Caracola flow includes (1) a broad shear area indicating distributed damage and intact granules in an extraction; (2) a large pore breakdown, often accompanied by small intracranial cracks caused by "fragmentation"; and (3) fractures. Unlike this distributed pervasive flow, the standard fragile deformation at low-effective pressures is characterized by an expansive fine fracture, leading to shear localization along narrower fracture zones, which often consist of sections linked to a zigzag pattern (e.g., [44–48]). In thin sections, the fragile fracture is evidenced by the presence of almost abundant small cracks, away from the shear fracture. Many of these miniature cracks are parallel to the main baseline pressure and may arise from axial splitting of healthy grains [42, 43] or cracking of grain boundaries.

From previous experimental studies, the researchers agreed that distributed sedimentary rocks, for calcarenitic sedimentary rocks, are the dominant failure mechanisms in highly porous rocks, especially at high effective medium pressures [49–52]. On the contrary, the fragile local fracture dominates the rocks with low porosity, as well as in high-porosity rocks with low effective pressure.

10. Conclusions

The catacombs of the Kom El-Shoqafa and Amod El-Sawari (Pompeii's pillar) site, located in the city center, 2.5 km from the sea coastline, are carved into the initial sandy limestone (cement limestone); Cross joints filled with fragmented sand and saturated with water in the lower parts. This unit is illustrated with loose sandstone. It is medium brown in color to decorate granulated limestone saturated with groundwater. It goes beyond the formation of the hayf (Pliocene) or the older myosin. Surface quadruple deposits obscure actual contact. The other two archeological sites, which are located close to the waterfront of Alexandria (Shatby Cemeteries, Mustafa Kamel Cemeteries), were excavated in internal limestone or calcite (coastal hills). Yellowish white upward become yellow brown bottom.

Based on tests carried out on air-dried samples prepared in the vertical direction, UCS values indicate that according to the classification adopted by the London Geological Society, which relies on the unrestricted compressive strength and the classification proposed by [33, 50]. These calcarenitic rocks from which excavations are carried out underground are classified as soft to very weak. It is also in good compliance with the Rock Quality Assignment System (RQD) for these types of soft rocks, where RR = 18 and RQD = 15–20% and a very poor quality range from 0 to 25. In addition, the results of static deformation tests indicate that the types of rock in question have high deformation.

It should be noted that the silica content at the Catacomb site in Kom El-Shoqafa is higher than in any area in Alexandria, possibly due to sedimentation processes, such as the high silica content that does not contain cement but is found as sand grains. In low rock durability and stiffness, high sand-like grain content reduces rock strength against salt crystallization and moisture pressures within rock pores. This is not only because of its high content of silica granules but also because it is a sparse rock. It is known that this type of limestone is characterized by low durability.

Three stages of crawling behavior can be identified by uniaxial and triple-axis crawling tests. In some cases, the primary creep curve approaches a constant rate of

stress called secondary creep. In high-stress specimens, secondary crawl may turn up in higher creep, which is characterized by an increased stress rate until crawl failure occurs suddenly. In the last two stages, the thin vertical cracking begins, accompanied by hardening, and only near failure, large cracks spread rapidly and lead to a sudden collapse. Long-term tests were performed on a secondary creep sample showing even at 40% of estimated strength.

The weathering process is associated with structural properties, such as poor geotechnical properties, carbon chemical composition, the presence of soluble salts in the porous system, marine climate with characteristic humidity, and marine spray, groundwater.

Author details

Sayed Hemeda
Conservation Department, Faculty of Archaeology, Cairo University, Egypt

*Address all correspondence to: sayed.hemeda@cu.edu.eg

IntechOpen

References

[1] Berest P, Charpentier JP, Blum PA. Creep of rock under small loading. In: Proceedings of SMRI Fall Meeting; Washington DC; 1999. pp. 11-24

[2] Costin LS. Time-dependent deformation and failure. In: Atkinson BK, editor. Fracture Mechanics of Rock. San Diego, CA: Academic; 1987. pp. 167-215

[3] Das S, Scholz CH. Theory of time-dependent rupture. Journal of Geophysical Research. 1981;**86**: 6039-6051

[4] De Meer A, Spiers CJ. Creep of wet gypsum aggregates under hydrostatic loading conditions. Tectonophysics. 1995;**245**:171-183

[5] ASTM D 4406–93 (Reapproved 1998). Standard test method for creep of cylindrical rock core specimens in triaxial compression; 1998. pp. 1-5

[6] Aydan IT, Zbay U, Kwasniewski M, Shariar K, Okuno T, Zgenoglu A, et al. ISRM suggested methods for determining the creep characteristics of rock. Rock Mechanics and Rock Engineering. 2014;**47**:275-290

[7] Bieniawski ZT. Mechanism of brittle fracture of rock. International Journal of Rock Mechanics and Mining Sciences. 1967;**4**:395-430

[8] Dusseault MB, Fordham CJ. Time dependent behaviour of rocks. Comprehensive Rock Engineering. 1993; **3**:119-149

[9] Hemeda S. Engineering failure analysis and design of support system for ancient Egyptian monuments in Valley of the Kings, Luxor, Egypt. Geoenvironmental Disasters. 2018;**5**:12. DOI: 10.1186/s40677-018-0100-x

[10] Haupt M, Natau O. Uniaxial relaxation test on rock salt. In: Proceedings of the 2nd Conference on Mechanical Behaviour of Salt; Hanover; 1984. pp. 180-185

[11] Ladanyi B. Time dependent response of rock around tunnels. Comprehensive Rock Engineering. 1993; **2**:77-112

[12] Lama RD, Vutukuri VS. Handbook on Mechanical Properties of Rocks-Testing Techniques and Results. Vol. 21978. pp. 209-323

[13] Maranini E, Brignoil M. Technical note: Creep behaviour of a weak rock: Experimental characterization. International Journal of Rock Mechanics and Mining Sciences. 1999;**36**:127-138

[14] Nomikos. Supported axisymmetric tunnel within linear viscoelastic burger rocks. Rock Mechanics and Rock Engineering. 2011;**44**:553-564

[15] Pan YW, Dong JJ. Time-dependent tunnel convergence I. Formulation of the model. International Journal of Rock Mechanics and Mining Science and Geomechanics Abstracts. 1991;**28**:477-488

[16] Robertson EC. Creep of Solenhofen limestone under moderate hydrostatic pressure. Geological Society of America Memoirs. 1963;**79**:227-244

[17] Wang Y, Qi J, Yang C, Wei J. A study of nonlinear creep law in deep rocks. Rock and Soil Mechanics. 2005;**26** (1):117-121

[18] Zhu H, Ye B. Experimental study on properties of rock creep in saturation. Chinese Journal of Rock Mechanics and Engineering. 2002;**21**(12):1791-1796

[19] Zhang Z, Luo J. Study on creep properties of rock under step load. Chinese Journal of Rock Mechanics and Engineering. 2004;**23**(2):218-222

[20] Liu J, Yang C, Li X, Jiang D. Testing study on creep of coal rocks in the tunnel of Wankai speedway. Chinese Journal of Rock Mechanics and Engineering. 2004;**23**(22):3794-3798

[21] Parkin AK. Creep of rockfill (Part A). In: Maranhadas Neves E, editor. Advances in Rockfill Structure. London: Kluwer Academic Publishers; 1992. pp. 221-239

[22] Shen Z, Zhao K. Back analysis of creep deformation of rockfill dams. Journal of Hydraulic Engineering. 1998; **6**:1-6

[23] Guo X, Wang D, Cai X, Dong L. Rheological analysis of concrete faced rock-fill dam. Journal of Hydraulic Engineering. 1999;**11**:42-46

[24] Wang M, He X, Cheng Z. Current situation and prospect of studies on rheology property of course stuff. Rock and Soil Mechanics. 2003;**Suppl**: 451-454

[25] Liu Y, Li Y, Sun M. A new method of permeability test for loose rock. Ground Pressure and Strata Control. 2002;**19**(4):108-110

[26] Hemeda S. An integrated approach for the pathology assessment and protection of underground monuments in seismic regions. Application on some Greek-Roman Monuments in Alexandria, Egypt [PhD thesis]. Greece: Aristotle University of Thessaloniki; 2008

[27] Hemeda S, Pitlakis K. Serapeum temple and the ancient annex daughter library in Alexandria, Egypt: Geotechnical-geophysical investigations and stability analysis under static and seismic conditions. Engineering Geology. 2010;**113**:33-43

[28] Hemeda S, Pitilakis K, Bandis S, Papayianni I, Gamal M. The Underground monuments (Catacombs) in Alexandria, Egypt. In: Proceedings of the 4th International Conference on Earthquake Geotechnical Engineering; Thessaloniki, Greece; 25–27 June, 2007. pp. 715-738

[29] Bieniawski ZT. The geomechanics classification in rock engineering applications, In: Proceedings of the Fourth International Conference on Rock Mechanics, Vol. 2. Montreox: ISRM; 1979. pp. 41-48

[30] Aydan O, Akagi T, Ito T, Kawamoto T. Prediction of behaviour of tunnels in squeezing ground. Journal of JSCE. 1992;**440**(3–9):73-82

[31] Aydan O, Akagi T, Kawamoto T. The squeezing potential of rocks around tunnels: Theory and prediction. Rock Mechanics and Rock Engineering. 1993; **26**(2):137-163

[32] Aydan O, Kawamoto T. The stability assessment of a large underground opening at great depth. In: 17th International Mining Congress and Exhibition of Turkey (IMCET 2001); Ankara, Vol. 1; 2001. pp. 277-288

[33] Aydan O, Ulusay R. Geotechnical and geo-environmental characteristics of man-made underground structures in Cappadocia, Turkey. Engineering Geology. 2003;**69**:245-272

[34] Aydan O, Ulusay R, Kawamoto T. Assessment of rock mass strength for underground excavations. In: The 36th US Rock Mechanics Symposium; 1997. pp. 777-786

[35] Deere DU, Varde OA. General report, engineering geological problems related to foundations and excavations in weak rocks. In: Proceedings of the 5th International Association of Engineering Geology Congress, 1986. Vol. 4. Balkema; 1990. pp. 2503-2518

[36] Hemeda S. 3D finite element coupled analysis model for geotechnical

and complex structural problems of historic masonry structures: conservation of Abu Serga church, Cairo, Egypt. Heritage Science. 2019;**7**:6. DOI: 10.1186/s40494-019-0248-z

[37] Hemeda S. Geotechnical and geophysical investigation techniques in Ben Ezra Synagogue in Old Cairo area, Egypt. Heritage Science. 2019;**7**:23. DOI: 10.1186/s40494-019-0265-y

[38] Hemeda S, Pitilakis K. Geophysical Investigations at Cairo's Oldest, the Church of Abu Serga (St. Sergius), Cairo, Egypt. Research in Nondestructive Evaluation. 2017;**28**(3): 123-149. DOI: 10.1080/09349.847.2016.11439.91

[39] Bukovansky M, Richard DP, Week KR. Influence of slope deformations on the tombs in the valley of the kings, Egypt. In: Engineering Geology and the Environment-Proceedings-Symposium; Athens, Vol. 3; 1997. pp. 3077-3080

[40] Berest P, Charpentier JP, Blum PA, Gharbi H. Very slow creep tests on rock samples. International Journal of Rock Mechanics and Mining Sciences. 2005; **42**:569-576

[41] Brace WF, Kohlstedt DL. Limits of lithospheric stress imposed by laboratory experiments. Journal of Geophysical Research. 1980;**85**:6348-6352

[42] Brace WF, Paulding BW, Scholz CH. Dilatancy in the fracture of crystalline rocks. Journal of Geophysical Research. 1958;**71**:3939-3953

[43] Charles RJ. Fatigue of glass, I. Journal of Applied Physics. 1966;**29**: 1549-1560

[44] Adachi T, Oka F. An elasto-plastic constitutive model for soft rock with strain softening. International Journal for Numerical and Analytical Methods in Geomechanics. 1995;**19**:233-247

[45] Arces M, Nocilla, Aversa S, Lo Cicero G. Geological and geotechnical features of the "Calcarenite di Marsala". In: Evangelista, Picarelli, editors. Proceedings of the Geotechnics of Hard Soils-Soft Rocks. Rotterdam: Balkema; 1998

[46] Atkinson BK. Introduction to fracture mechanics and its geophysical applications. In: Atkinson BK, editor. Fracture Mechanics of Rocks. San Diego, CA: Academic; 1987. pp. 1-26

[47] Atkinson BK, Meredith PG. The theory of sub-critical crack growth with applications to minerals and rocks. In: Atkinson BK, editor. Fracture Mechanics of Rocks. San Diego, CA: Academic; 1987. pp. 111-166

[48] Aversa S. Mechanical behaviour of soft rock: Some remarks. In: Proceedings of the Workshop on "Experimental Characterization and Modelling of Soil and Soft Rocks. Napoli; 1991. pp. 191-223

[49] Aydan O, Tokashiki N, Kawamoto T. Microstructure models for porous rocks to jointed rock masses. In: Third Asia-Pacific Conference on Computational Mechanics; Seoul, Vol. 3; 1996. pp. 2235-2242

[50] Cecconi M, Viggiani G. Physical and structural properties of a pyroclastic soft rock. In: Evangelista, Picarelli, editors. Proceedings of the Geotechnics of Hard Soils-Soft Rocks. Rotterdam: Balkema; 1998

[51] Cooper MR. The mechanics of uncemented carbonate sands. Geotechnique. 1990;**40**(4):607-627

[52] Cripps JC, Coulthard JM, Forster A, Hencher SR, Moon CF. The engineering geology of weak rock. In: Proceedings of the 26th Annual Conference of the Engineering Group of the Geological Society, Leeeds (AA Balkema, Engineering Geology Special Publication, 8); 1993. 510pp